Electronic Supplementary Material (ESI) for Reaction Chemistry & Engineering.

Supporting Information

Catalyst and Reactor Design Considerations for Selective Production of Acids by Oxidative Cleavage of Alkenes and Unsaturated Fatty Acids with H_2O_2

Danim Yun, Zhongyao Zhang and David W. Flaherty*

DOE Center for Advanced Bioenergy and Bioproducts Innovation, University of Illinois at Urbana-Champaign
Department of Chemical and Biomolecular Engineering, University of Illinois at Urbana-Champaign, Urbana, Illinois 61801

*Corresponding Author

Phone: (217) 244-2816

Email: dwflhrty@illinois.edu

S1.0. Synthesis and Characterization of the WO_x-Al_2O_3 Catalyst

S1.1. WO_x-Al_2O_3 Catalyst Synthesis

Aluminum oxide (γ-Al_2O_3, Sigma Aldrich; 3.8 nm pores, 364 $m^2 \cdot g^{-1}$) was calcined in flowing air (Airgas, Ultra Zero Grade) at 823 K for 6 h to remove organic residues and moisture. The cooled solid (~1 g) was added to chloroform (80 cm^3; $CHCl_3$, TCI Chemical, ≥99.0%) in a two-neck round-bottom flask under Ar (Airgas, 99.999%) flow in a glass air-free apparatus. The mixture was stirred for 0.5 h (300 rpm, ~295 K), after which the designated amount of bis(cyclopentadienyl)tungsten dichloride ($(C_5H_5)_2WCl_2$, Alfa Aesar, 99%) was added as a dry powder to a suspension of alumina in $CHCl_3$. The mixture was stirred under continuous Ar purge for 0.5 h. Three equivalents of triethylamine ($(C_2H_5)_3N$, Sigma-Aldrich, 99.5%) were added to the mixture to deprotonate sites surface hydroxyls and adsorb $(C_5H_5)_2WCl_2$. The mixture was stirred for another 12 h. Subsequently, the solids were filtered, dried, and calcined at 823 K for 6 h in flowing air (100 $cm^3 \cdot min^{-1}$; Airgas, Ultra Zero Grade) to form tungsten oxide complexes (WO_x) on the alumina. The resulting WO_x-Al_2O_3 materials were characterized (*vide infra*) by EDXRF and adsorption and desorption isotherms of N_2. The mass loading and the areal density of W atoms on the Al_2O_3 support for the WO_x-Al_2O_3 catalyst are 3.6% and 0.4 $W \cdot nm^{-2}$, respectively.

S1.2. Characterizaiton of WO_x-Al_2O_3 Catalyst

Adsorption and desorption isotherms of N_2 were performed using a Micrometrics 3Flex analyzer and SmartVac degasser. Catalyst (< 50 mg) was loaded into a glass vessel and heated under vacuum to desorb water and organic residues. The degassed sample was weighed and the isotherms were then obtained. The N_2 adsorption-desorption isotherm of γ-Al_2O_3 calcined at 823 K for 6 h shows a type IV isotherm with H1-type hysteresis. The total surface areas of these samples were determined to be 281 $m^2 \cdot g^{-1}$ using the BET method.

In situ Raman spectroscopy was used to examine the structure of tungsten oxide domains in the dehydrated catalysts. Raman spectra of the dehydrated catalysts were obtained from catalyst pellets placed in an environmentally controlled high-temperature cell reactor (Linkam, CCR1000). Before analysis, the catalysts were dehydrated at 823 K for 1 h in flowing O_2 (Airgas, ultrahigh purity, 20 cm^3 min^{-1}) to desorb adsorbed moisture. The spectra were collected after cooling the catalyst to room temperature under flowing O_2 gas (20 cm^3 min^{-1}). Spectra were acquired with a Raman spectrometer (Renishaw, inVia) equipped with a 532 nm laser at less than 41 $mW \cdot \mu m^{-2}$ at the catalyst surface. The power density was measured directly using a portable power meter (Gentec-EO, PRONTO-Sl).

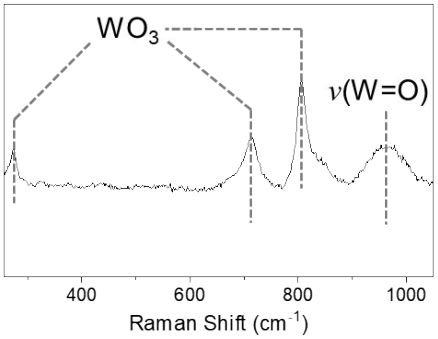

Fig. S1 *In situ* Raman spectra of WO_x-Al_2O_3 under dry flowing helium (298 K, 101 kPa He) after dehydration (773 K, 1 h, 20 $cm^3 \cdot min^{-1}$). Reprinted (adapted) with permission from D. Yun *et al.*, ACS Catal. 2021, 11, 5, 3137–3152. Copyright 2022 American Chemical Society.

Figure S1 shows steady-state Raman spectra of the catalysts under dehydrated condition. Raman spectra of dehydrated WO_x-Al_2O_3 contains features at 274, 719, 809, assigned to δ(O−W−O), ν(W−O), and ν(O−W−O) modes, respectively, of the monoclinic WO_3 structure,[S1] and 953 cm^{-1} correspond to the ν(W=O) of distorted monotungstate.[S2,S3] The results suggest that the WO_x-Al_2O_3 catalyst contains oligomeric tungstate surface species and WO_3 aggregates under dehydrated condition.

S2.0. Concentration profiles of the reactant and the products after separating the heterogeneous catalyst from the reaction solution or after cooling down the reaction solution with homogeneous catalyst to room temperature

S2.1. Concentration profiles of 4-octene, 4,5-epoxyoctane, and butanal in the reaction solution with homogeneous catalysts during a reaction and after cooling it down to room temperature

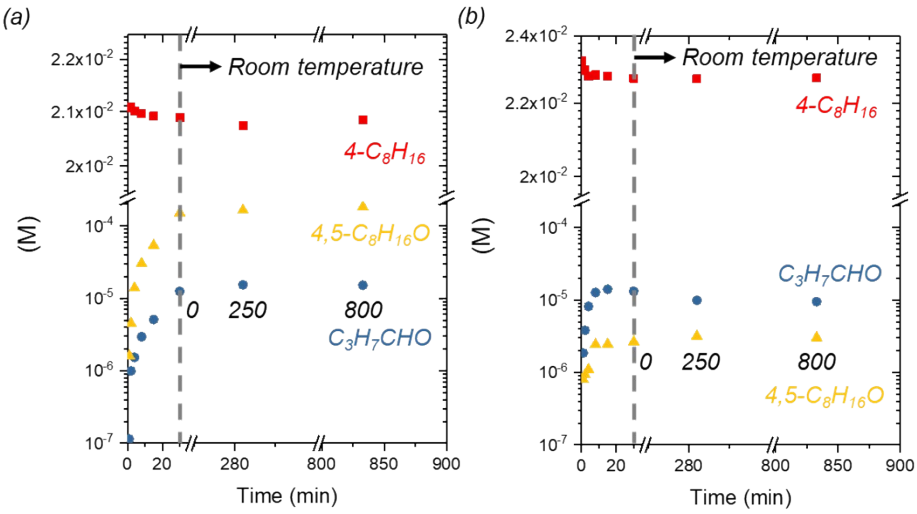

Fig. S2 4-Octene, 4,5-epoxyoctane, and butanal concentrations in the reaction solutions during a reaction (21 to 23 mM 4-C_8H_{16}, 0.1 M H_2O_2, and 0.39 M H_2O in CH_3CN) with (a) H_2WO_4 and (b) W-POM catalysts at 333 K, and after cooling to room temperature, as a function of time

Figure S2 shows that the reactant and the products concentrations are nearly constant in the reaction solutions after cooling to room temperature. Thus, we assume that the oxidative cleavage reaction with homogeneous catalysts ends once the temperature reaches room temperature.

S2.2. Hot Filtration Test

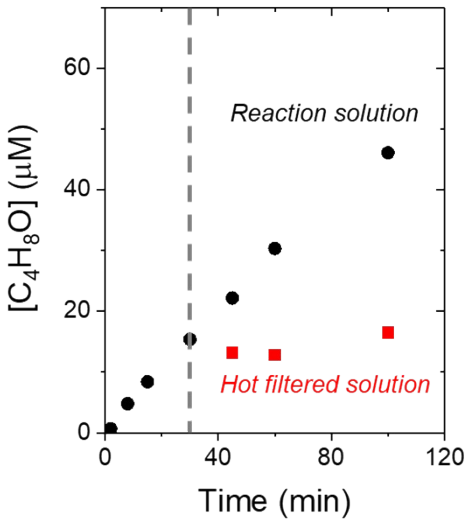

Fig. S3 Butanal concentrations of (●) non-filtered reaction solution and (■) hot filtered solution as a function of reaction time (22 mM 4-C_8H_{16}, 0.1 M H_2O_2, 0.39 M H_2O in CH_3CN) over WO_x-Al_2O_3 at 333 K

To determine if catalytically active forms of WO_x leach from the alumina support, we carried out hot filtration tests for WO_x-Al_2O_3 catalyst. Hot filtered solutions do not show any change in butanal concentration (Figure S3), indicating that active WO_x species do not leach from the alumina support under theses conditions, and the oxidative cleavage reaction with heterogeneous catalysts ends once the catalyst is separated from the reaction solution.

.

S3.0. Derivation of reactor design and component generation rate equations in the oxidative cleavage of 4-octene

S3.1. Reactor Design Equations

We assumed that mass transfer is negligible, and there is one homogeneous phase in a batch or semibatch reactor due to vigorous stirring. In the case of the semibatch reactor, the volumes were assumed additive, which implies that a simple update formula for the liquid volume (V_L) is applied,

$$V_L = V_{0L} + V't \tag{S1}$$

where V_{0L} is the initial volume and V' is the volumetric flow rate of aqueous hydrogen peroxide solution. The mass balance equation for an arbitrary component can be written as

$$n'_{0i} + r_i m_{cat} = \frac{dn_i}{dt} \tag{S2}$$

where n'_{0i} is the molar flow rate of component i in the feed ($n'_{0i} \neq 0$ for hydrogen peroxide and water, but $n'_{0i} = 0$ for the other components), n_i is the moles of substance i in the reactor and mcat is the mass of the catalyst. The term r_i denotes the catalytic generation rate of the component i. The moles of substance (n_i) can be elaborated further, because $n_i = C_i V_L$. Differentiation gives:

$$\frac{dn_i}{dt} = \frac{d(C_i V_L)}{dt} = \frac{dC_i}{dt} V_L + C_i \frac{dV_L}{dt} \tag{S3}$$

According to Equation (S1), $dV_L/dt = V'$. After inserting these relations into the balance Equation (S3), the mass balance becomes

$$\frac{dC_i}{dt} V_L + C_i \frac{dV_L}{dt} = C_{0i} V' + r_i m_{cat} \tag{S4}$$

$$\frac{dC_i}{dt} = (C_{0i} - C_i)\frac{V'}{V_L} + r_i \frac{m_{cat}}{V_L} \tag{S5}$$

Equation (S5) describes the changes of the concentrations of semibatch components.

For a batch reaction, there is no liquid volume change (e.g. $V_L = V_{0L}$, V'=0) and all component concentrations in the feed are zero (e.g. $n'_{0i} = 0$). Therefore, the mass balance and the reactor design equations are, respectively:

$$r_i m_{cat} = \frac{dn_i}{dt} \tag{S6}$$

$$\frac{dC_i}{dt} = r_i \frac{m_{cat}}{V_{0L}} \tag{S7}$$

Equation (S7) describes the changes of the concentrations of batch components.

S3.2. Component generation rates

a. Oxidative cleavage of alkenes

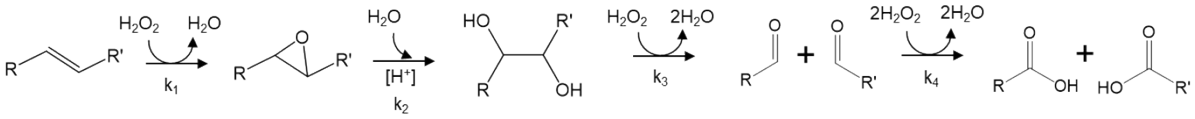

b. Decomposition of hydrogen peroxide

$$H_2O_2 \xrightarrow[k_5]{} H_2O + 1/2O_2$$

Scheme 1. Stoichiometric reactions involved in the oxidative cleavage of alkenes with H_2O_2 and decomposition of H_2O_2.

For the oxidative cleavage reaction, the generation rates of each component are obtained as linear combinations of r_1 through r_5. Therefore, the generation rates for each component are:

$$r_{4-C_8H_{16}} = -r_1 \quad \text{(S8)}$$

$$r_{4,5-C_8H_{16}O} = r_1 - r_2 \quad \text{(S9)}$$

$$r_{4,5-C_8H_{16}(OH)_2} = r_2 - r_3 \quad \text{(S10)}$$

$$r_{C_3H_7CHO} = 2r_3 - r_4 \quad \text{(S11)}$$

$$r_{C_3H_7COOH} = r_4 \quad \text{(S12)}$$

$$r_{H_2O_2} = -r_1 - r_3 - r_4 - r_5 \quad \text{(S13)}$$

S4.0. W content confirmation

S4.1. Atomic W confirmation in the reaction mixture after oxidative cleavage of oleic acid with H_2O_2 on homogeneous catalyst

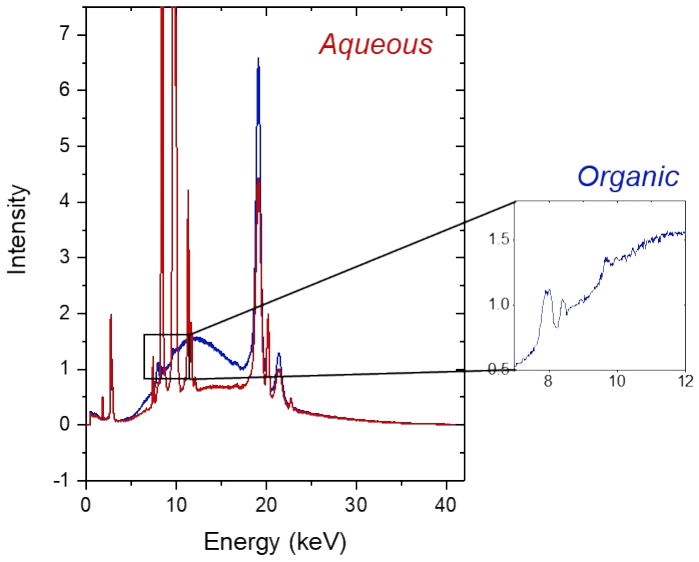

Fig. S4 EDXRF signals for the organic (blue) and aqueous phases (red) of the oxidative cleavage reaction mixture (0.95 M OA, 6.85 M H_2O_2, 27.1 M H_2O, 343 K) on W-POM catalyst

Figure S4 shows EDXRF spectra of the organic and aqueous phases of the reaction mixture when we use W-POM as a catalyst. Except the peaks attributed to Rh and Cu originating from the laser source, the peaks at 8.4, 9.7, and 10 keV can be attributed to W L_α, W $L_\beta 1$, and W $L_\beta 2$, respectively. Most of W-POM catalyst is dissolved in the aqueous phase after the reaction (92%) and a small amount of W-POM remains in the organic phase (0.3%), indicating that complete separation of the homogeneous catalysts from the reaction mixture is challenging.

S4.2. Atomic W confirmation in the used WO_x-Al_2O_3 catalysts as a function of H_2O_2 concentration

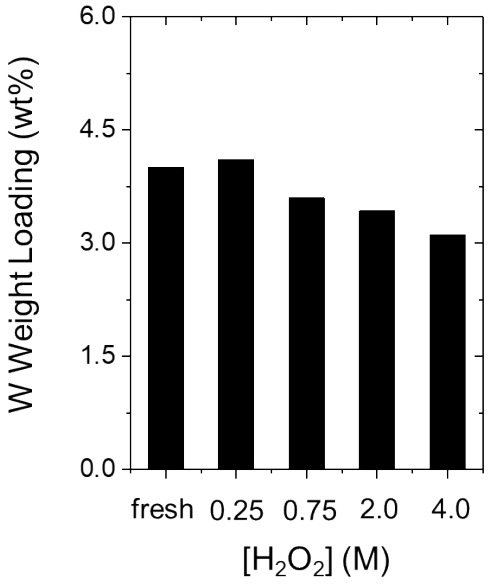

Figure S5. W weight loading of fresh and used WO_x-Al_2O_3 catalysts after the H_2O_2 treatment (0.25-4 M H_2O_2, 1-16 M H_2O in CH_3CN, 333 K, 1 h) measured by EDXRF

We measured the quantity of W atoms remaining upon the Al_2O_3 following contact with H_2O_2 solutions of different concentrations (0.25–4.00 M H_2O_2, 1–16 M H_2O in CH_3CN) at 333 K for 1 h. The W atom content remains unchanged when [H_2O_2] remains equal to or lower than 0.25 M H_2O_2, but increasingly quantities of W atoms leach from the support as [H_2O_2] increases from 0.75 M (10% W lost) to 4.0 M (22% W lost).

S4.3. Regeneration of WO_x-Al_2O_3 catalyst in batch and semibatch operations

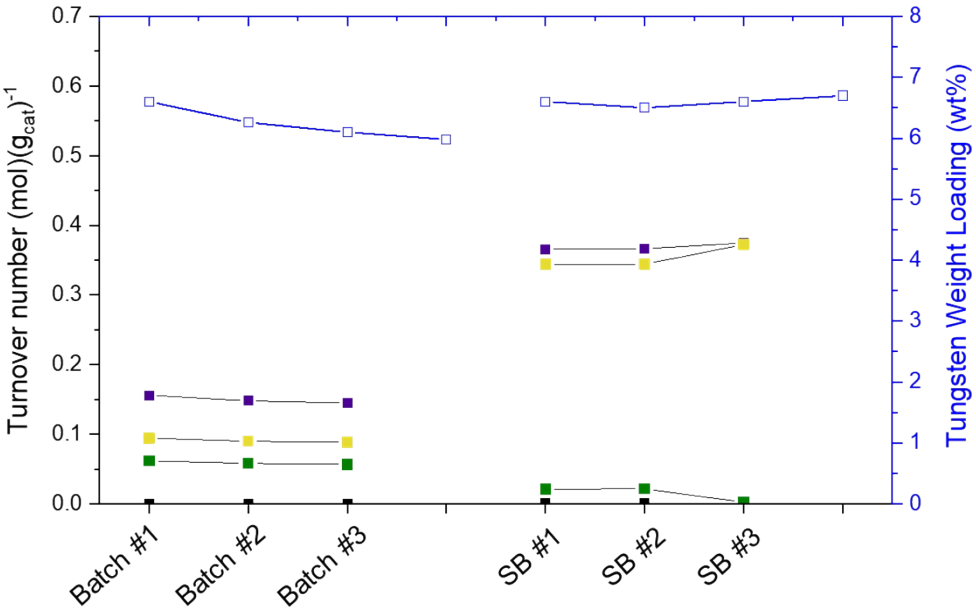

Figure S6. Tungsten weight loading of fresh and regenerated WO_x-Al_2O_3 catalysts and turnover number for for consumed alkenes (■) and formed epoxides (■), diols (■), and oxidative cleavage products (■, aldehydes and acids) during recycle test (50 mM 4-octene, 0.5 M H_2O_2, 1.98 M H_2O in CH_3CN, 333K for batch or 50 mM 4-octene in CH_3CN, 333K, F_{H2O2}=1.3 µL min^{-1} for semibatch operations) over WO_x-Al_2O_3.

To confirm the reusability of WO_x-Al_2O_3 catalyst in batch and semibatch operations, we conducted four subsequent reactions. EDXRF results show that 9.4% of W leaches from the support after three sequential BSTR operation (50 mM 4-octene, 0.5 M H_2O_2, 1.98 M H_2O in CH_3CN, 333K), while W does not leach from the Al_2O_3 after SBR operation (50 mM 4-octene in CH_3CN, 333K, F_{H2O2}=1.3 µL min^{-1}).The turnover numbers slightly decrease (~7%) after three sequential BSTR operation, but turnover numbers consistently manintain for all three semibatch reactions. This demonstrates that the WO_x-Al_2O_3 catalysts are stable and regenerable during semibatch operation.

S5.0. Derivation of ratio of oxidative cleavage rate to H_2O_2 decomposition rate over tungstates and [M-H_2O_2*] formed by H_2O_2 adsorption and activation on empty active site

S5.1. Derivation of Rate Expressions for the oxidative cleavage of alkene with H_2O_2 and H_2O_2 decomposition over tungstates

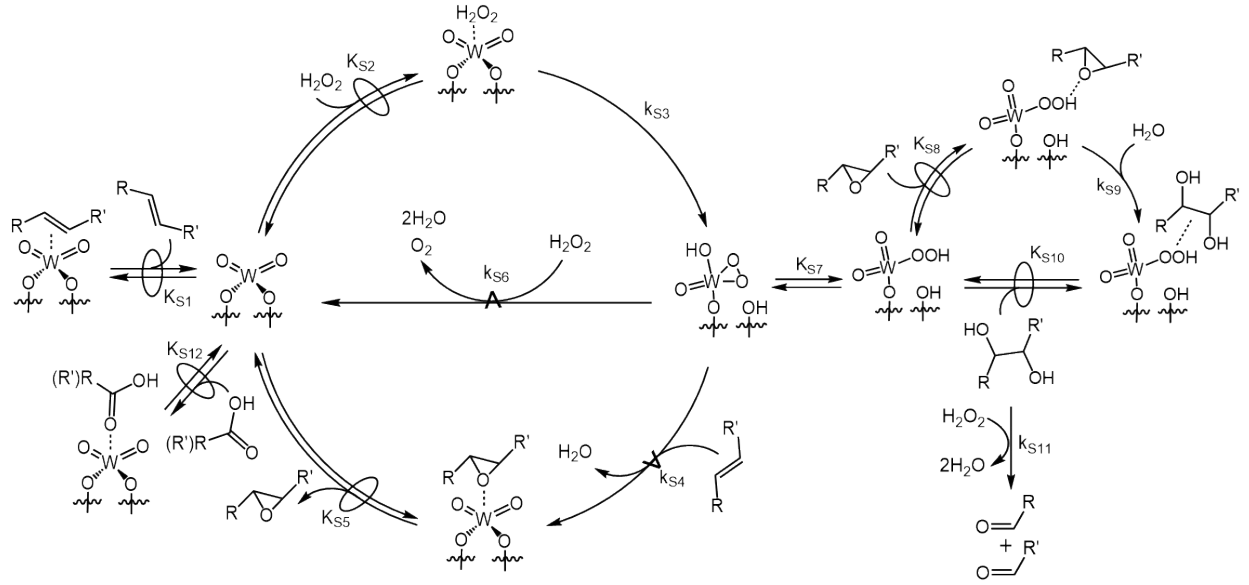

Scheme S2. Proposed mechanism for oxidative cleavage of alkene with H_2O_2 and H_2O_2 decomposition over tungstates. The ⇳ symbol denotes a quasi-equilibrated step and the ⇗ symbol signifies the kinetically relevant steps for the formation of distinct products. Reprinted (adapted) with permission from D. Yun *et al.*, ACS Catal. 2021, 11, 5, 3137–3152. Copyright 2022 American Chemical Society.

Scheme S2 illustrates a series of elementary steps beginning with the quasi-equilibrated adsorption of alkene (step S1) and hydrogen peroxide, H_2O_2 (step S2) which is followed by the irreversible activation of H_2O_2 to form M-(η^2-O_2) (step S3). Activation of H_2O_2 can result in H_2O_2 decomposition (step S6) or kinetically relevant epoxidation (step S4) by reacting with a H_2O_2 molecule or alkene molecule, respectively. The epoxyoctane desorbs in a quasi-equilibrated manner (step S5) and Brønsted acids of W-OOH complexes protonate and bind the epoxide. Subsequently, the protonated intermediate reacts with water to irreversibly hydrolyze the epoxide and form the epoxyoctanediol (step S9), which desorbs (step S10). Finally, the epoxyoctanediol is converted to an alpha-hydroxy ketone intermediate by reaction with the basic solvent and then cleaves the C-C bonds following nucleophilic attack of H_2O_2 in the liquid-phase (step S11).

The epoxidation of 4-octene represents the kinetically relevant step that determines rates of oxidative cleavage

$$r_{OC} = k_{S4}\left[W-(\eta^2-O_2)\right]\left[C_8H_{16}\right] \tag{S14}$$

Applying the pseudo-steady state hypothesis to W-(η2-O2) and W-OOH intermediates, produces Equation S15:

$$\frac{d[W-(\eta^2-O_2)]}{dt} \approx 0 = k_{S3}\left[H_2O_2*\right] - k_{S4}\left[C_8H_{16}\right]\left[W-(\eta^2-O_2)\right] - k_{S6}\left[H_2O_2\right][W-(\eta^2-O_2)] \tag{S15}$$

where k_{Sx} represents the rate constant for step Sx, [W-(η^2-O_2)] is the number of W-(η^2-O_2) and W-OOH, [H_2O_2*] is the number of H_2O_2 molecules bound to active sites, and all other species within brackets ([]) are the corresponding

liquid-phase concentrations. When H_2O_2 adsorption is assumed to be quasi-equilibrated (step S2, Scheme S1), Equation S14 can be rearranged to yield:

$$[W-(\eta^2-O_2)] = \frac{k_{S3}K_{S2}[H_2O_2][*]}{k_{S4}[C_8H_{16}]+k_{S6}[H_2O_2]} \tag{S16}$$

where [*] is the number of unoccupied (or solvent-covered) active sites. This equation is then combined with equation (S14) to yield

$$\frac{r_{OC}}{[L]} = \frac{\dfrac{k_{S3}k_{S4}K_{S2}[4-C_8H_{16}][H_2O_2]}{k_{S4}[4-C_8H_{16}]+k_{S6}[H_2O_2]}}{1+K_{S1}[4-C_8H_{16}]+K_{S2}[H_2O_2]+\dfrac{k_3K_2[H_2O_2]}{k_{S4}[4-C_8H_{16}]+k_{S6}[H_2O_2]}+\dfrac{[4{,}5-C_8H_{16}O]}{K_{S5}}+K_{S11}[C_4H_8O]+K_{S12}[C_4H_8O_2]} \tag{S17}$$

where [L] is the total number of active sites and K_{Sx} is the equilibrium constant for step Sx in Scheme S1. The five terms in the denominator signify the numbers of sites that are occupied by CH_3CN, 4-C_8H_{16}, H_2O_2, W-(η^2-O_2) and W-OOH, 4,5-$C_8H_{16}O$, butanal, and butanoic acid, respectively.

Similarly, the reaction between W-(η^2-O_2) and H_2O_2 determines H_2O_2 decomposition rates (r_D)

$$r_D = k_{S6}\,[H_2O_2][W-(\eta^2-O_2)] \tag{S18}$$

The application of pseudo-steady state hypothesis on [W-(η^2-O_2)] leads to equation S18 to be restated as:

$$\frac{r_D}{[L]} = \frac{\dfrac{k_{S3}k_{S6}K_{S2}[H_2O_2]^2}{k_{S4}[4-C_8H_{16}]+k_{S6}[H_2O_2]}}{1+K_{S1}[4-C_8H_{16}]+K_{S2}[H_2O_2]+\dfrac{k_{S3}K_{S2}[H_2O_2]}{k_{S4}[4-C_8H_{16}]+k_{S6}[H_2O_2]}+\dfrac{[4{,}5-C_8H_{16}O]}{K_{S5}}+K_{S11}[C_4H_8O]+K_{S12}[C_4H_8O_2]} \tag{S19}$$

From equations S17 and S19, the rate ratio of oxidative cleavage to H_2O_2 decomposition is obtained:

$$\frac{r_{OC}}{r_D} = \frac{\dfrac{k_{S3}k_{S4}K_{S2}[4-C_8H_{16}][H_2O_2]}{k_{S4}[4-C_8H_{16}]+k_{S6}[H_2O_2]}}{\dfrac{k_{S3}k_{S6}K_{S2}[H_2O_2]^2}{k_{S4}[4-C_8H_{16}]+k_{S6}[H_2O_2]}} = \frac{k_{S4}[4-C_8H_{16}]}{k_{S6}[H_2O_2]} \tag{S20}$$

S5.2. Derivation of [H_2O_2-M*] for the H_2O_2 adsorption and activation on metals

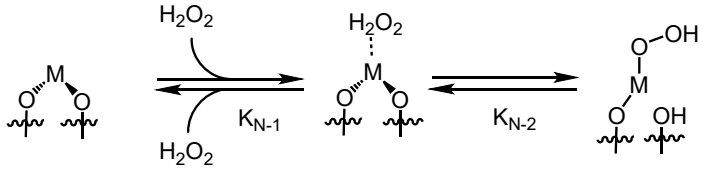

Scheme S3 The H_2O_2 activation mechanism on metals.

Scheme S3 illustrates elementary steps equilibrating adsorption (step N-1) and activation (step N-2) of H_2O_2 on the metal sites. The concentration of H_2O_2-adsorbed site ([H_2O_2*]) is relating to the fractional occupancy of H_2O_2 onto the empty active sites, and the equilibrium reaction between empty site (*) and H_2O_2-adsorbed site (H_2O_2*) yields Equation S21:

$$[H_2O_2*] = \frac{K_{N-1}[H_2O_2]}{1 + K_{N-1}[H_2O_2]} \tag{S21}$$

Where K_{H1} is the equilibrium constant for step N-1 in Scheme S2.

Similarly, the equilibrium reaction between H_2O_2-adsorbed site (H_2O_2*) and H_2O_2-activated metal site (H_2O_2-M*) gives Equation S22:

$$[H_2O_2 - M*] = \frac{K_{N-2}[H_2O_2*]}{1 + K_{N-2}[H_2O_2*]} \tag{S22}$$

Equation (S21) is substituted into Equation (S22) provides Equation S23:

$$[H_2O_2 - M*] = \frac{K_{N-1}K_{N-2}[H_2O_2]}{1 + (K_{N-2} + 1)K_{N-1}[H_2O_2]} \tag{S23}$$

We can assume that the activation of H_2O_2 (step N-2) is irreversible ($K_{N-2} \gg 1,\ K_N = K_{N-1}K_{N-2}$), which yields Equation S24:

$$[H_2O_2 - M*] = \frac{K_{N-1}K_{N-2}[H_2O_2]}{1 + K_{N-1}K_{N-2}[H_2O_2]} = \frac{K_N[H_2O_2]}{1 + K_N[H_2O_2]} \tag{S24}$$

S5.3. Derivation of [W-(η^2-O_2)] for the H_2O_2 adsorption and activation on W

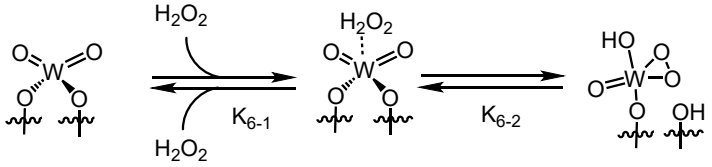

Scheme S4 The H_2O_2 activation mechanism on W to form W-(η^2-O_2).

In the similar way (S21 through S24) in S5.2, we obtain Equation S25 with the assumption that H_2O_2 is activated on W sites irreversibly.

$$\left[W-(\eta^2-O_2)\right] = \frac{K_{6-1}K_{6-2}[H_2O_2]}{1+K_{6-1}K_{6-2}[H_2O_2]} = \frac{K_6[H_2O_2]}{1+K_6[H_2O_2]} \quad \text{(S25)}$$

S5.4. Derivation of [W-OOH] for the H_2O_2 adsorption and activation on W

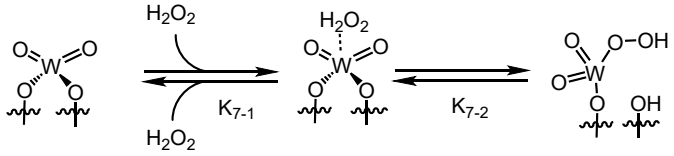

Scheme S5 The H_2O_2 activation mechanism on W to form W-OOH.

In the similar way (S21 through S24) in S5.2, we obtain Equation S26 with the assumption that H_2O_2 is activated on W sites irreversibly.

$$[W-OOH]=\frac{K_{7-1}K_{7-2}[H_2O_2]}{1+K_{7-1}K_{7-2}[H_2O_2]}=\frac{K_7[H_2O_2]}{1+K_7[H_2O_2]} \quad \text{(S26)}$$

S5.5. Derivation of [H_2O_2-W(or Al)*] for the H_2O_2 adsorption and activation on W or Al sites

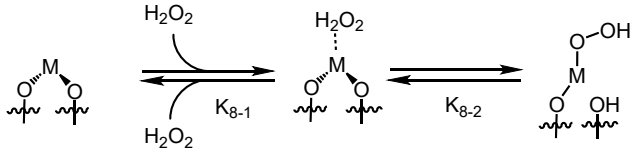

Scheme S6 The H_2O_2 activation mechanism on W or Al metals (M in scheme S6 is W or Al).

In the similar way (S21 through S24) in S5.2, we obtain Equation S27 with the assumption that H_2O_2 is activated on W or Al sites irreversibly.

$$\left[H_2O_2 - W(or\ Al) *\ \right] = \frac{K_{8-1}K_{8-2}[H_2O_2]}{1 + K_{8-1}K_{8-2}[H_2O_2]} = \frac{K_8[H_2O_2]}{1 + K_8[H_2O_2]} \quad \text{(S27)}$$

S6.0. Initial rate measurements for step reactions

S6.1. Ring-opening of 1,2-epoxyoctane

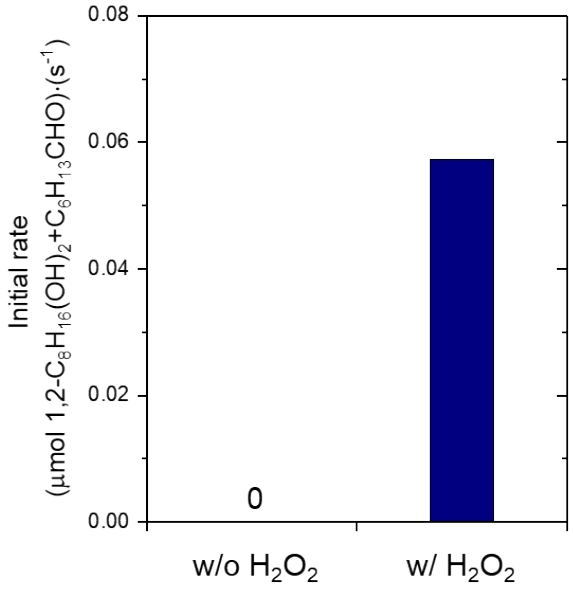

Fig. S7 Initial rates for ring-opening of 1,2-epoxyoctane (0.025 M 1,2-$C_8H_{16}O$, 0.1 M or 0 M H_2O_2, 0.39 M H_2O in CH_3CN at 333 K) over WO_x-Al_2O_3 (mass loading of W is 0.5 %). Reprinted (adapted) with permission from D. Yun *et al.*, ACS Catal. 2021, 11, 5, 3137–3152. Copyright 2022 American Chemical Society.

Figure S6 shows the initial rates for the ring-opening of 1,2-epoxyoctane with H_2O_2 and H_2O or in the absence of H_2O_2 over WO_x-Al_2O_3 catalyst (mass loading of W is 0.5 %). The ring-opening of 1,2-epoxyoctane does not show measurable rates in the absence of H_2O_2, which suggests this step reaction occurs on H_2O_2-activated W sites. The H_2O_2-activated complexes on W-containing catalysts include W-peroxo (W-(η^2-O_2)) and W-hydroperoxo (W-OOH), and Brønsted acid sites are known to activate epoxide for the ring-opening reaction. The W-OOH sites, therefore, are plausible active sites for this step.

S6.2. Oxidative cleavage of 1,2-octanediol

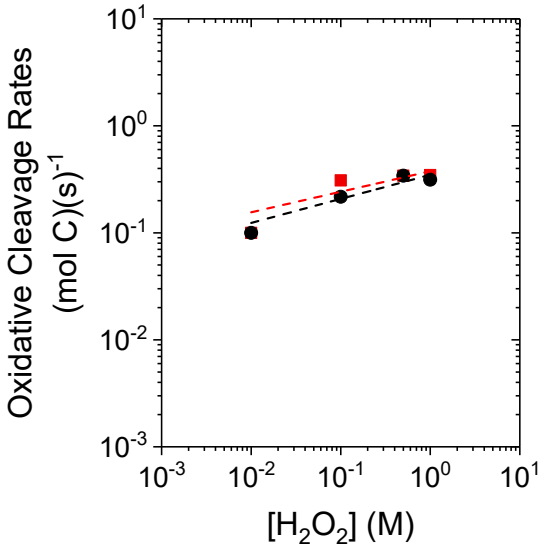

Fig. S8 Oxidative cleavage rates (heptanal and heptanoic acid formation rates) in the oxidative cleavage of 1,2-octanediol (0.03 M 1,2-$C_8H_{16}(OH)_2$ in CH_3CN at 333 K) as a function of $[H_2O_2]$ on WO_x-Al_2O_3 (●) or in the absence of the catalyst (■)

Figure S7 shows oxidative cleavage rates by oxidative cleavage of 1,2-octanediol as a function of concentration of H_2O_2. The rates of heptanal and heptanoic acid formations were used to report oxidative cleavage rates. The measured rates does not depend on the presence of the catalyst, which suggests this reaction occurs by liquid H_2O_2 in aqueous CH_3CN. This agrees with proposals by Venturello et al. They described that alpha-hydroxy ketone is formed followed by C-C bond cleavage of diol by nucleophilic attack of H_2O_2. The measured rates do not depend on the $[H_2O_2]$, which means that the production of an alpha-hydroxy ketone represents the kinetically relevant step that determines the oxidative cleavage rates of 1,2-octanediol.

S6.3. H_2O_2 decomposition

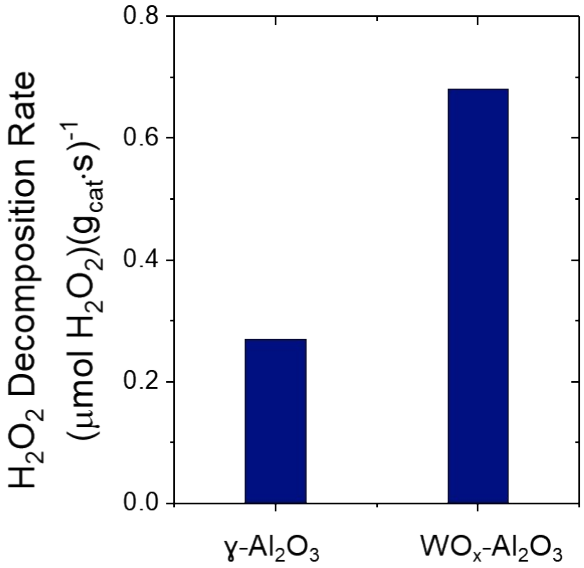

Fig. S9 H_2O_2 decomposition rates (10 mM H_2O_2, 39 mM H_2O in CH_3CN, 333 K) over γ-Al_2O_3 and WO_x-Al_2O_3 (mass loading of W is 0.5 %). Reprinted (adapted) with permission from D. Yun *et al.*, ACS Catal. 2021, 11, 5, 3137–3152. Copyright 2022 American Chemical Society.

Figure S8 shows the turnover rates for H_2O_2 decomposition on γ-Al_2O_3 and WO_x-Al_2O_3 (mass loading of W is 0.5 %) catalysts. The measured rates show that both γ-Al_2O_3 and WO_x-Al_2O_3 decomposes H_2O_2 to form water and molecular oxygen.

S7.0 parity and residual plots

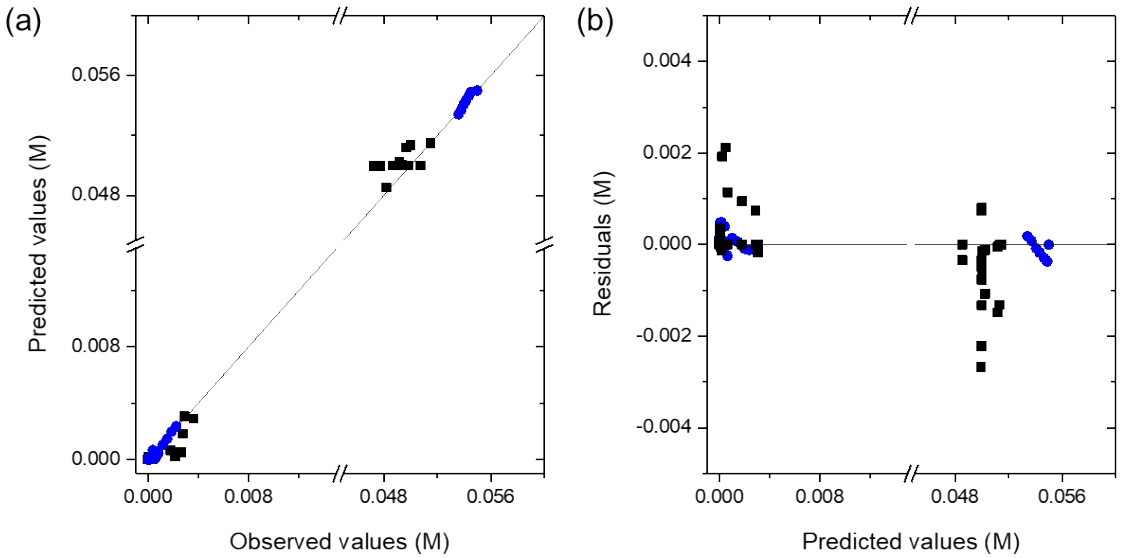

Fig. S10 (a) Parity and (b) redisual plots for batch (●) and semi-batch (■) operations

Figure S10 shows parity and residual plots for batch and semi-batch operations, which supports that the kinetic model describes in a well manner the experimental data.

S8.0 Semibatch prediction results

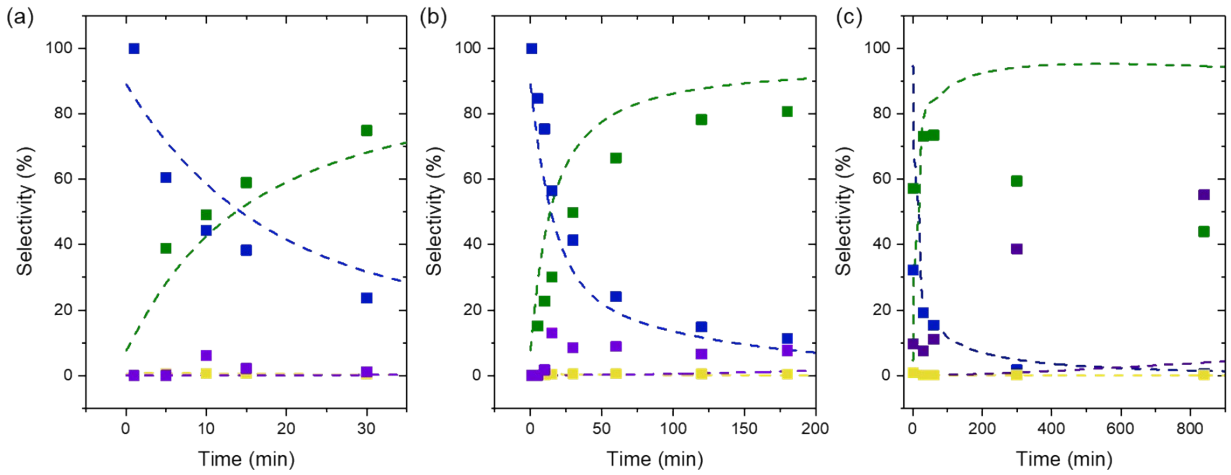

Fig. S11 Oxidative cleavage (0.05 M 4-octene in CH_3CN at 333 K) products (4,5-epoxyoctane (■), 4,5-octanediol (■), butanal (■), butanoic acid (■)) selectivities as a function of time under semibatch conditions (F_{H2O2}= (a) 51, (b) 8.5, and (c) 1.3 μL min^{-1}): model prediction (dashed lines) and experimental data (scatter) for WO_x-Al_2O_3 catalyst.

Figure S9 compares the model prediction and experiment data for oxidative cleavage products selectivities as a function of time under the different feed rate of H_2O_2 (F_{H2O2}) in the semibatch operation. Decrease of F_{H2O2} from 51 to 1.3 ul min^{-1} increases oxidative cleavage product (the sum of butanal and butyric acid) selectivities from 70 to 99%. When we decrease F_{H2O2} to 1.3 ul min^{-1}, we can see that a good fit was accomplished except the error for estimation of the oxidation of butanal to butyric acid. The possible reasons for that is explained in the manuscript section 3.4.

S9.0 Modeling Code

```
%% Optimizing

k_ini = [2.8;502;50000;38.5;110;5000;50000;1000]' ;

options = optimoptions('fmincon','Display','iter','Algorithm','sqp', 'MaxIterations',1500,...
   'StepTolerance',1e-12,  'MaxFunEvals',1e3,'TolX',1e-25,'TolFun',1e-25,'DiffMinChange',1e-1);

k_opt = fmincon(@(k) fn_opt2(k, m_cat, fit_ii, C_i_ini), k_ini, [], [], [], [], ...
   [0.28;50.2;5000;3.85;11.0;500;5000;100], [280;5020;500000;385;1100;50000;500000;10000], ...
   [], options) ;

[obj, CC, ts] = fn_opt2(k_opt, m_cat, fit_ii, C_i_ini) ;
```

References

(S1) R.F. Garcia-Sanchez, T. Ahmido, D. Casimir, S. Baliga, and P. Misra, *J. Phys. Chem. A*, 2012, **117 (50)**, 13825−13831.

(S2) N. Maity, S. Barman, Y. Minenkov, S. Ould-Chikh, E. Abou-Hamad, T. Ma, Z. S. Qureshi, L. Cavallo, V. D'Elia, and B. C. Gates *ACS Catal.* 2018, **8 (4)**, 2715−2729.

(S3) E. L. Lee and I. E. Wachs, *J. Phys. Chem. C* 2007, **111 (39)**, 14410−14425.